JOURNAL OF APPLIED PHYSICS **116**, 223706 (2014)

Electronic and thermoelectric properties of InN studied using *ab initio* density functional theory and Boltzmann transport calculations

P. D. Borges[a),b)] and L. Scolfaro[a)]
Department of Physics, Texas State University, San Marcos, Texas 78666, USA

(Received 5 August 2014; accepted 29 November 2014; published online 11 December 2014)

The thermoelectric properties of indium nitride in the most stable wurtzite phase (w-InN) as a function of electron and hole concentrations and temperature were studied by solving the semiclassical Boltzmann transport equations in conjunction with *ab initio* electronic structure calculations, within Density Functional Theory. Based on maximally localized Wannier function basis set and the *ab initio* band energies, results for the Seebeck coefficient are presented and compared with available experimental data for *n*-type as well as *p*-type systems. Also, theoretical results for electric conductivity and power factor are presented. Most cases showed good agreement between the calculated properties and experimental data for w-InN unintentionally and *p*-type doped with magnesium. Our predictions for temperature and concentration dependences of electrical conductivity and power factor revealed a promising use of InN for intermediate and high temperature thermoelectric applications. The rigid band approach and constant scattering time approximation were utilized in the calculations. © *2014 AIP Publishing LLC*.
[http://dx.doi.org/10.1063/1.4904086]

I. INTRODUCTION

Indium nitride and its alloys with Al and Ga are important materials for applications in light-emitting diodes, lasers, transistors, and solar-cells.[1–7] Compared to the other group III-nitrides, InN has the smallest effective mass, highest electron mobility, and least dependence of band gap energy on temperature. By using molecular beam epitaxy (MBE), it is possible to produce InN samples with high quality, where important quantities such as the free electron concentrations and electron mobility have been well-established. As direct consequence, an appropriate measurement of the band gap was obtained at 300 K, with the value of 0.64 eV.[6] Recently, InN, InGaN, and AlInN have also been a subject of investigation as promising thermoelectric (TE) materials, with the aim of being integrated with high-power III-nitride based device technologies.[7–14]

The rapid increase in the world's energy demand has driven the intense research recently seen in the field of alternative and sustainable energies. TE materials have attracted great attention due to their ability of both generating electrical energy from a heat source and solid state cooling, therefore contributing to improved energy efficiency through waste heat recovery and more effective cooling. The effectiveness of a material for TE applications is determined by the dimensionless figure of merit, $ZT = \sigma S^2 T/\kappa$, where S is the Seebeck coefficient, σ is the electrical conductivity, T is the absolute temperature, and κ is the thermal conductivity. In order to achieve more efficient TE devices, it is critical to maximize ZT. High values of figure of merit require high values of S and σ and low κ. The difficulty found to increase ZT lies in the fact that as S increases σ decreases. Moreover, an increase in σ leads to an increase in κ. The power factor of a TE material is given by $P = \sigma S^2$, which involves all the important electrical properties of the material. The recent reports of transport and TE properties of group-III nitrides have shown values for the Seebeck coefficient and power factor which are encouraging and will drive more studies towards further improvement of ZT.[11–28] Despite the fact that there are some experimental reports on transport and TE properties of InN, no detailed theoretical study of these properties based on *ab initio* electronic structure calculations, combined with the solution of Boltzmann transport equations has been reported so far. In this work, we present the results of theoretical predictions of transport and thermoelectric properties of w-InN obtained within the semiclassical Boltzmann transport theory, using a maximally localized Wannier function (MLWF) and band structure calculations based on Density Functional Theory (DFT).

II. COMPUTATIONAL METHODS

All calculations were carried out by using the DFT and the Generalized Gradient Approximation (GGA) for the exchange-correlation term.[29] Band structures and density of states were obtained by employing the Projector Augmented Wave method as implemented in the Vienna *Ab-initio* Simulation Package (VASP-PAW) within a full-relativistic approach, including the spin-orbit coupling effects.[30–32] The importance of relativistic effects in the group-III nitrides has been reported by us in a previous work.[33] The modified Becke-Johnson exchange potential (mBJ),[34,35] which greatly improves band gap accuracy has also been used in conjunction with the VASP package. For w-InN, the valence electronic distribution for the PAWs representing the atoms were In $4d^{10}\ 5s^2\ 5p^1$ and N $2s^2\ 2p^3$. A $4 \times 4 \times 4$ Monkhorst-Pack[36] k-points mesh have been adopted for the Brillouin

[a)]Electronic addresses: pdborges@gmail.com and lscolfaro@txstate.edu
[b)]Permanent address: Instituto de Ciências Exatas e Tecnológicas, Universidade Federal de Viçosa, 38810-000 Rio Paranaiba, MG, Brazil.

zone integrations. All the calculations were performed with a 400 eV energy cutoff in the plane-wave expansions. The calculations were done for the experimental hexagonal *wurtzite* crystal structure ($P6_3mc$ - #186) with lattice constants, $a = 3.533$ Å and $c = 5.693$ Å. The crystal structure was relaxed until the residual forces on the ions were less than 10 meV/Å.

The transport calculations were done using Boltzmann transport theory within the constant scattering time (τ) approximation recently implemented in the BoltzWann code, using a MLWF basis set to interpolate the band structure obtained from first-principles calculations.[37] This approximation for τ is based on the assumption that the scattering time determining the electrical conductivity does not vary considerably with energy on the scale of k_BT. It does not implicate any assumption about the possible doping and temperature dependence of τ. The benefit of using this approximation is that the Seebeck coefficient, S(T), is calculated without adjustable parameters. After using a $4 \times 4 \times 4$ k-points grid for the construction of the MLWFs, a $40 \times 40 \times 40$ mesh was utilized to calculate the transport properties. For 22 MLWFs around the gap region, we applied the disentanglement procedure, through which entangled bands can be separated, and we were able to reproduce the valence bands (VBs) as well as lowest-energy conduction states.[37,38] We choose the frozen window energy equal to the calculated Fermi energy. The Wannier-functions interpolated band structure showed excellent agreement with the first-principles results.

The following expressions were used for the transport tensors for the electrical conductivity σ and Seebeck coefficient S as a function of the chemical potential μ and of the temperature T:[37]

$$[\sigma]_{ij}(\mu, T) = e^2 \int_{-\infty}^{+\infty} dE \left(-\frac{\partial f(E, \mu, T)}{\partial E} \right) \sum_{ij}(E), \quad (1)$$

$$[\sigma S]_{ij}(\mu, T) = \frac{e}{T} \int_{-\infty}^{+\infty} dE \left(-\frac{\partial f(E, \mu, T)}{\partial E} \right) (E - \mu) \sum_{ij}(E), \quad (2)$$

where i and j are Cartesian indices, σS denotes the matrix product of the two tensors, $\partial f/\partial E$ is the derivative of the Fermi–Dirac distribution function with respect to the energy and the transport distribution function

$$\Sigma_{ij}(E) = \frac{1}{V} \sum v_i(n,k) v_j(n,k) \tau_{nk} \delta(E - E_{n,k}) \quad (3)$$

considers the summation over all bands n and in the whole Brillouin zone. $E_{n,k}$ is the energy for band n at k, τ_{nk} is the scattering time, which is held constant with respect to an electron on band n at wavevector k, and $v_i = \hbar^{-1} \partial E_{n,k}/\partial k_i$ is the i-th component of the band velocity at (n, k). Within this approximation, the Seebeck coefficient is independent of τ_{nk} that drops off from Eq. (2). As a consequence, in some cases, S can be under- or overestimated, since the relaxation time is not a constant, and depends on scattering processes. Nevertheless, approximation is the most successful approach for solving the Boltzmann equation. In Eq. (1), the scattering time is a multiplicative factor and, therefore, just promoting a rigid shift on the electrical conductivity behavior. All expressions presented above are implemented in the BoltzWann code.[37]

III. RESULTS

In Fig. 1 are shown the calculated band structure for w-InN with (a) and without (b) the mBJ correction in the exchange potential, where for the former a negative band gap of ~0.05 eV was obtained. After taking into consideration, the mBJ correction (Fig. 1(a)), a band gap equal to 0.65 eV was found which shows excellent agreement with experimental results (0.6–0.7 eV).[39–45] Other calculations performed beyond the local density approximation (LDA) or using modified LDA potentials have shown values for the InN band gap in the range of 0.58–0.88 eV.[46–51] Fig. 1(a) shows a good agreement between the band structure of w-InN obtained through first-principles calculations (solid line) and the Wannier functions (WFs) interpolation using 22 WFs (circles).

For the transport calculations, it is important to have a good band gap value as well as to take into account both the valence and conduction band (CB) non-parabolicity. Both conditions were fulfilled from the *ab initio* calculations including the mBJ correction and from the WFs calculations.

The total and projected densities of states are shown in Fig. 2. The lowest energy states lying between −15.5 eV and −11.0 eV depict In(d) and N(s) atomic orbital character. The higher VB states located around −5 eV–0 eV are composed of a mixture of In(s), (p) and (d), and N(p) atomic character. The lower lying CB states show a mixing character of In(s), (p) and N(s), N(p).

In Fig. 3, our theoretical results are compared with experimental data[12–14] for the Seebeck coefficient S *versus* electron concentration n for a set of n-type InN samples, not intentionally doped, in the range of 10^{17}–10^{21} cm^{-3} at room temperature. Due to the strong dependence of the effective

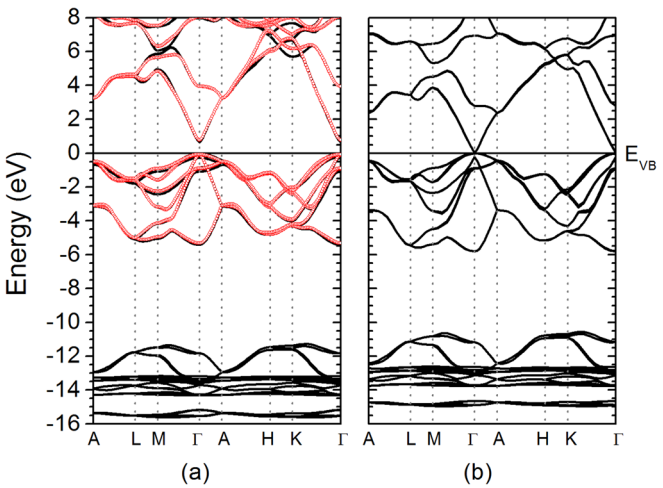

FIG. 1. Calculated band structure for w-InN (a) with and (b) without the inclusion of the mBJ correction for the exchange potential with a band gap energy 0.65 eV and 0.05 eV, respectively. The band structure obtained from the Wannier functions interpolation is shown between −6 eV and 8 eV (red circles).

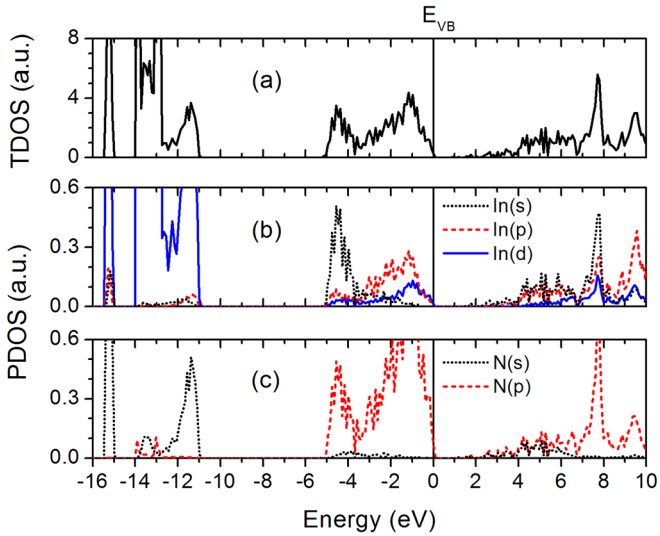

FIG. 2. (a) The total and (b), (c) projected densities of states of w-InN. The top of the VB is taken as the energy zero (E_{VB}), and is indicated by a vertical solid line.

mass on electron concentration, we adopted here the value $m_e^*/m_0 = 0.05$ (Ref. 52) to determine the effective density of states.[53] We observe a good agreement between the data and the theoretical predictions for S at low concentrations ($<10^{19}\,cm^{-3}$). Dislocation defects play an important role on the transport properties of InN.[13,14] If the effect of dislocations are taken into account as a fraction of the total n, we can estimate the influence of carrier concentration upon Seebeck coefficient. Considering a higher fraction 49% ($N_{dis} = 0.49n$), we observe a small downward shift of the S curve, when compared with that with no-N_{dis}. For higher concentrations ($>10^{19}\,cm^{-3}$), both curves deviate from the experimental data. Included also in Fig. 3 is the Seebeck coefficient versus concentrations, as plotted in non-degenerate ($S_{n\text{-deg}}$) and degenerate (S_{deg}) limits for which the relationship between momentum relaxation time (τ) and energy (E) is a power law function ($\tau \propto E^r$)[53]

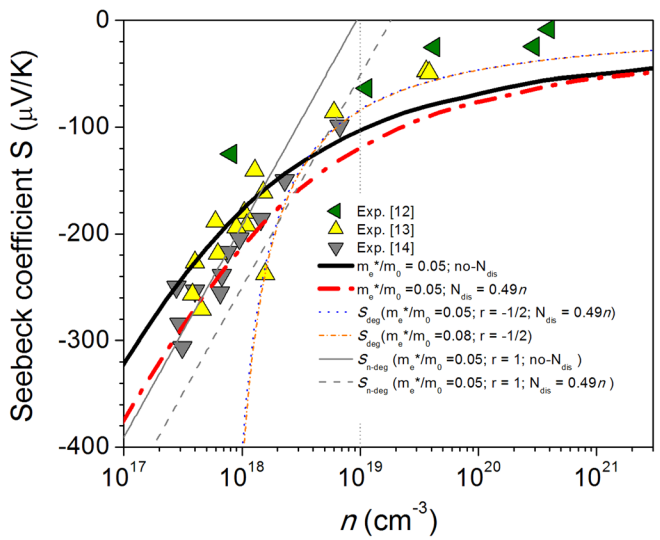

FIG. 3. Theoretical (thick lines) and experimental (symbols) results for Seebeck coefficient versus free electron concentration in the range of 10^{17}–$10^{21}\,cm^{-3}$ at room temperature. Theoretical curves were obtained using BoltzWann code, in which the actual band structure energies are used as input. Experimental data were extracted from Refs. 12 to 14. Electron effective mass values were only used to determine the effective density of states. We also show results for Seebeck coefficients in the degenerate (S_{deg}) and non-degenerate ($S_{n\text{-deg}}$) limits, obtained from Eqs. (4) and (5). The vertical dotted line indicates the non-degenerate to degenerate behavior boundary.

$$S_{n-\text{deg}} = \frac{k_B}{e}\left(r + \frac{5}{2} - \frac{\zeta}{k_B T}\right), \tag{4}$$

$$S_{\text{deg}} = \frac{k_B}{e}\left(r + \frac{3}{2}\right)\frac{\pi^3}{3}\frac{k_B T}{\zeta}, \tag{5}$$

where k_B is the Boltzmann constant, e is the electron charge, r is the power law index in the relaxation time and ζ is the Fermi energy, relative to the band edge. Using Eq. (4), a good fitting is observed for low concentrations, which fails for higher concentrations. On the other hand, when Eq. (5), including dislocations effects, is utilized a better fitting is seen for high concentrations. These results indicate a transition from a non-degenerate to a degenerate limit behavior around $n = 10^{19}\,cm^{-3}$. For $n < 10^{19}\,cm^{-3}$ and $n > 10^{19}\,cm^{-3}$ we found, respectively, r = 1 and r = −1/2 indicating that the electron scattering is dominated by phonons or ionized impurities.[12] When dislocations were taken into account in the non-degenerate limit the curve shows a small downward shift and a discrepancy is observed for low concentrations, in spite of being in reasonable agreement for samples with $n \approx 10^{19}\,cm^{-3}$. Strong influence of dislocations has been seen by Miller and co-workers[13] for a sample with $n = 6 \times 10^{18}\,cm^{-3}$. In the degenerate limit, a similar behavior is observed between the curves obtained considering an effective mass value of $0.08m_0$,[52] without take into account dislocations explicitly, or considering an effective mass value of $0.05m_0$ and $N_{dis} = 0.49n$. Therefore, since the effective mass is strongly dependent on concentration in w-InN,[52] a suitable value of m* is sufficient to describe the behavior of n, at least in a certain range.

Experimental data[11,13] together with our theoretical results for T-dependent Seebeck coefficient for p-type and n-type InN are shown in Figs. 4(a) and 4(b), respectively. Varying the Fermi level energy (E_F) close to the bottom of the conduction band (E_{CB}) we obtain a good agreement between theoretical and experimental results for three n-type samples with electron concentrations 4×10^{17}, 9×10^{17}, and $6 \times 10^{18}\,cm^{-3}$. Miller and co-workers studied Mg-doped InN films grown by MBE (Ref. 11) and obtained p-type films as evidenced by a positive Seebeck coefficient. By varying E_F close to the top of the valence band (E_{VB}), we were able to fit the experimental results. For the sample with Mg concentration $p_{Mg} = 2 \times 10^{18}\,cm^{-3}$, a deviation is observed for $T > 250\,K$. In this case, a fitting using Eqs. (4) and (5) was not possible. A better agreement is obtained for the sample with $p_{Mg} = 6 \times 10^{18}\,cm^{-3}$, showing a strong dependence of the Seebeck coefficient on the concentration. By using Eq. (4) and assuming r = 0, we observe a similar behavior, which is an indicative of a non-degenerate behavior and momentum relaxation time independent of energy. In the p-type case, the calculated values of −0.437 eV and 0.169 eV for

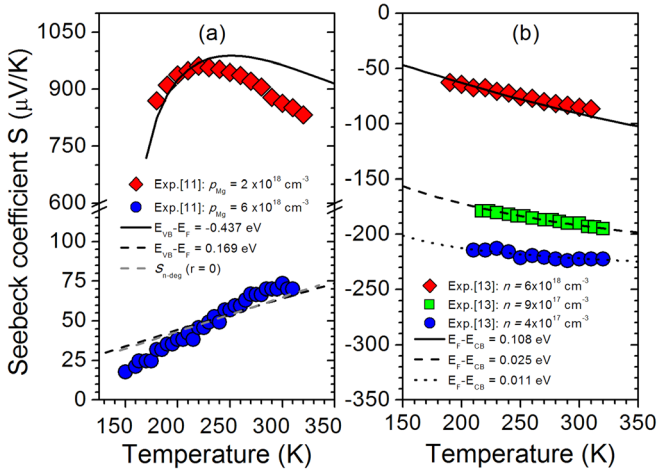

FIG. 4. Theoretical and experimental results for Seebeck coefficient versus temperature in the range of 125–350 K for w-InN in (a) *p*-type and (b) *n*-type conditions. Experimental data were extracted from Refs. 11 and 13. The calculated values for $E_{VB} - E_F = -0.437$ eV and 0.169 eV correspond, respectively, to 2×10^{18} cm^{-3} and 6×10^{17} cm^{-3} magnesium concentrations (p_{Mg}). For *n*-type, the values used for $E_F - E_{CB} = 0.108$ eV, 0.025 eV, and 0.011 eV correspond to 6×10^{18} cm^{-3}, 9×10^{17} cm^{-3}, and 4×10^{17} cm^{-3} free electron concentrations (n), respectively.

the Fermi energy, relative to the top of the valence band ($\zeta = E_{VB} - E_F$), correspond to 2×10^{18} cm^{-3} and 6×10^{17} cm^{-3} magnesium concentrations, respectively, even though these values did not represent directly the hole free concentrations. For *n*-type, the values of 0.108 eV, 0.025 eV, and 0.011 eV were used for the Fermi energy, relative to the bottom of the conduction band ($\zeta = E_F - E_{CB}$), corresponding, respectively, to 6×10^{18} cm^{-3}, 9×10^{17} cm^{-3}, and 4×10^{17} cm^{-3} free electron concentrations.

In Figs. 5(a) and 5(b), we show the calculated Seebeck coefficient as a function of free carrier concentration calculated at 300 K, 500 K, 700 K, and 900 K. A value of $0.05 m_0$ for the electron effective mass was assumed for *n*-type.[52] We observe a decrease in *S* while *n* increases, but in the whole range of electron concentrations the Seebeck coefficient

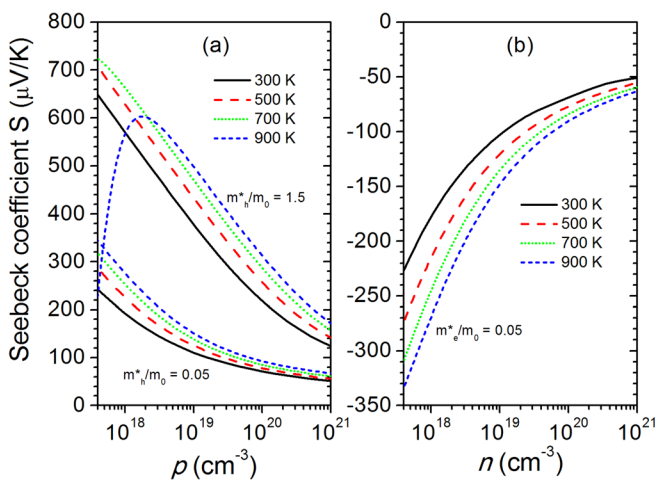

FIG. 5. Theoretical results for Seebeck coefficient *versus* free carrier concentration in the range of 10^{17}–10^{21} cm^{-3} for different temperatures. (a) *p*-type and (b) *n*-type conditions for w-InN. Carrier effective mass values are considered only to determine the effective densities of states.

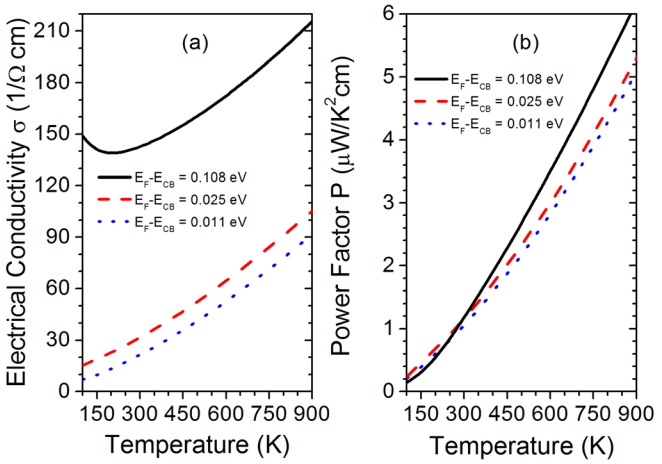

FIG. 6. Theoretical results for (a) electrical conductivity and (b) power factor versus temperature for three different concentrations in *n*-type conditions for w-InN. The calculated values 0.108 eV, 0.025 eV, and 0.011 eV for the Fermi energy, relative to the bottom of the conduction band, ($E_F - E_{CB}$), correspond to 6×10^{18}, 9×10^{17} cm^{-3}, and 4×10^{17} cm^{-3} free electron concentrations, respectively.

increases with temperature. For *p*-type, two different values for the hole effective mass were adopted in the calculations, 0.05 m_0 and 1.5 m_0, trying to account for the distinct hole bands. A strong dependence on m_h^* was observed for *S*. Similar to the *n*-type, a decreasing *S* behavior with the increase in free hole concentration (p) is seen, and in the entire range of p the Seebeck coefficient increases with temperature. A different behavior is observed for T = 900 K and m = 1.5 m_0, where S decreases for low concentrations.

The *T*-dependent electrical conductivity (σ) and power factor ($P = \sigma S^2$) are shown in Figs. 6(a) and 6(b), respectively, for the three *n*-type cases presented in Fig. 5(b). For the two cases with the lowest concentrations σ increases with temperature, with similar behavior and close values. A larger increase in σ is observed for higher n, whereas a decreasing in σ is seen for temperatures up to 200 K. The power factor increases in all cases between 100 and 900 K. Above 300 K, we observe that P increases with the increase in electron concentration. A suitable value for τ (= 10 fs) was used, in accordance with terahertz spectroscopy measures ($\tau < 50$ fs).[54] According to Eq. (1), a rigid shift in the σ and P curves is possible for different values of the scattering time.

IV. CONCLUSIONS

Using *ab initio* DFT calculations for the electronic structure including the mBJ correction to the exchange potential we obtained a suitable description of wurtzite InN, with a band gap energy value of 0.65 eV, in excellent agreement with experiment (0.6–0.7 eV). The *ab initio* band energies results, combined with the semiclassical Boltzmann transport theory, were applied to study the transport properties of InN using a maximally localized Wannier functions basis for band structures interpolation. A good agreement was shown between our theoretical results and the available experimental data for *n*- and *p*-type materials. We verified that an appropriate description for band structure together with the

rigid band approximation are powerful tools to study transport and thermoelectric properties of InN. Our predicted temperature and concentration dependences of electrical conductivity and power factor indicate that InN is a powerful candidate for intermediate and high temperature thermoelectric applications. Further improvement of thermoelectric features may be expected by engineering the structures such as the use of heterostructures or nanoinclusions involving InN and its alloys.

ACKNOWLEDGMENTS

This work was supported by the Brazilian funding agency CNPq and the Materials Science, Engineering, and Commercialization program at Texas State University. We also thank the suggestions made by Dr. C. Swartz from Texas State University.

[1]D. Queren, A. Avramescu, G. Brüderl, A. Breidenassel, M. Schillgalies, S. Lutgen, and U. Strau, Appl. Phys. Lett. **94**, 081119 (2009).
[2]J. Zhang, S. Kutlu, G. Liu, and N. Tansu, J. Appl. Phys. **110**, 043710 (2011).
[3]N. F. Gardner, G. O. Muller, Y. C. Shen, G. Chen, S. Watanabe, W. Gotz, and M. R. Krames, Appl. Phys. Lett. **91**, 243506 (2007).
[4]C. J. Neufeld, N. G. Toledo, S. C. Cruz, M. Iza, S. P. DenBaars, and U. K. Mishra, Appl. Phys. Lett. **93**, 143502 (2008).
[5]U. K. Mishra, P. Parikh, and Y. F. Wu, Proc. IEEE **90**, 1022 (2002).
[6]J. Wu, J. Appl. Phys. **106**, 011101 (2009) and references therein.
[7]D. Veal, C. F. McConville, and W. J. Schaff, *Indium Nitride and Related Alloys* (CRS Press/Taylor & Francis, London, 2009).
[8]H. Tong, J. Zhang, G. Liu, J. A. Herbsommer, G. S. Huang, and N. Tansu, Appl. Phys. Lett. **97**, 112105 (2010).
[9]G. Chen and A. Shakouri, J. Heat Transfer **124**, 242 (2002).
[10]A. Sztein, H. Ohta, J. E. Bowers, S. P. DenBaars, and S. Nakamura, J. Appl. Phys. **110**, 123709 (2011).
[11]N. Miller, J. W. Ager, H. M. Smith, M. A. Mayer, K. M. Yu, E. E. Haller, W. Walukiewicz, W. J. Schaff, C. Gallinat, G. Koblmüller, and J. S. Speck, J. Appl. Phys. **107**, 113712 (2010).
[12]A. X. Levander, T. Tong, K. M. Yu, J. Suh, D. Fu, R. Zhang, H. Lu, W. J. Schaff, O. Dubon, W. Walukiewicz, D. G. Cahill, and J. Wu, Appl. Phys. Lett. **98**, 012108 (2011).
[13]N. Miller, E. E. Haller, G. Koblmüller, C. Gallinat, J. S. Speck, W. J. Schaff, M. E. Hawkridge, K. M. Yu, and J. W. Ager III, Phys. Rev. B **84**, 075315 (2011).
[14]O. Bierwagen, S. Choi, and J. S. Speck, Phys. Rev. B **84**, 235302 (2011).
[15]J. Zhang, H. Tong, G. Liu, J. Herbsommer, G. S. Huang, and N. Tansu, J. Appl. Phys. **109**, 053706 (2011).
[16]B. N. Pantha, R. Dahal, J. Li, J. Y. Lin, H. X. Jiang, and G. Pomrenke, J. Electron. Mater. **38**, 1132 (2009).
[17]B. N. Pantha, R. Dahal, J. Li, J. Y. Lin, H. X. Jiang, and G. Pomrenke, Appl. Phys. Lett. **92**, 042112 (2008).
[18]W. Liu and A. A. Balandin, J. Appl. Phys. **97**, 073710 (2005).
[19]W. Liu and A. A. Balandin, J. Appl. Phys. **97**, 123705 (2005).
[20]A. Sztein, H. Ohta, J. Sonoda, A. Ramu, J. E. Bowers, S. P. DenBaars, and S. Nakamura, Appl. Phys. Express **2**, 111003 (2009).
[21]E. N. Hurwitz, M. Asghar, A. Melton, B. Kucukgok, L. Su, M. Orocz, M. Jamil, N. Lu, and I. T. Ferguson, J. Electron. Mater. **40**, 513 (2011).
[22]S. Yamaguchi, Y. Iwamura, and A. Yamamoto, Appl. Phys. Lett. **82**, 2065 (2003).
[23]N. Kaiwa, M. Hoshino, T. Yaginuma, R. Izaki, S. Yamaguchi, and A. Yamamoto, Thin Solid Films **515**, 4501 (2007).
[24]S. Yamaguchi, R. Izaki, N. Kaiwa, and A. Yamamoto, Appl. Phys. Lett. **86**, 252102 (2005).
[25]R. Izaki, N. Kaiwa, M. Hoshino, T. Yaginuma, S. Yamaguchi, and A. Yamamoto, Appl. Phys. Lett. **87**, 243508 (2005).
[26]S. Yamaguchi, R. Izaki, N. Kaiwa, S. Sugimura, and A. Yamamoto, Appl. Phys. Lett. **84**, 5344 (2004).
[27]S. Yamaguchi, R. Izaki, K. Yamagiwa, K. Taki, Y. Iwamura, and A. Yamamoto, Appl. Phys. Lett. **83**, 5398 (2003).
[28]G. Chen, M. S. Dresselhaus, G. Dresselhaus, J.-P. Fleurial, and T. Caillat, Int. Mater. Rev. **48**, 45 (2003).
[29]J. P. Perdew, K. Burke, and M. Ernzerhof, Phys. Rev. Lett. **77**, 3865 (1996).
[30]G. Kresse and D. Joubert, Phys. Rev. B **59**, 1758 (1999).
[31]G. Kresse and J. Furthmüller, Comput. Mater. Sci. **6**, 15 (1996).
[32]G. Kresse and J. Furthmüller, Phys. Rev. B **54**, 11169 (1996).
[33]L. E. Ramos, L. K. Teles, L. M. R. Scolfaro, J. L. P. Castineira, A. L. Rosa, and J. R. Leite, Phys. Rev. B **63**, 165210 (2001).
[34]A. D. Becke and E. R. Johnson, J. Chem. Phys. **124**, 221101 (2006).
[35]F. Tran and P. Blaha, Phys. Rev. Lett. **102**, 226401 (2009).
[36]H. Monkhorst and J. Pack, Phys. Rev. B **13**, 5188 (1976).
[37]G. Pizzi, D. Volja, B. Kozinsky, M. Fornari, and N. Marzari, Comput. Phys. Commun. **185**, 422 (2014).
[38]I. Souza, N. Marzari, and D. Vanderbilt, Phys. Rev. B **65**, 035109 (2001).
[39]S. X. Li, J. Wu, E. E. Haller, W. Walukiewicz, W. Shan, H. Lu, and W. J. Schaff, Appl. Phys. Lett. **83**, 4963 (2003).
[40]O. K. Semchinova, J. Aderhold, and J. Graul, Appl. Phys. Lett. **83**, 5440 (2003).
[41]J. Wu, W. Walukiewicz, W. Shan, K. M. Yu, J. W. Ager, S. X. Li, E. E. Haller, H. Lu, and W. J. Schaff, J. Appl. Phys. **94**, 4457 (2003).
[42]B. Arnaudov, T. Paskova, P. P. Paskov, B. Magnusson, E. Valcheva, B. Monemar, H. Lu, W. J. Schaff, H. Amano, and I. Akasaki, Phys. Rev. B **69**, 115216 (2004).
[43]J.-W. Yoon, S. S. Kim, H. Cheong, H.-C. Seo, S.-Y. Kwon, H.-J. Kim, Y. Shin, E. Yoon, and Y.-S. Park, Semicond. Sci. Technol. **20**, 1068 (2005).
[44]V. Yu. Davydov, A. A. Klochikhin, R. P. Seisyan, V. V. Emtsev, S. V. Ivanov, F. Bechstedt, J. Furthmüller, H. Harima, A. V. Mudryi, J. Aderhold, O. Semchinova, and J. Graul, Phys. Status Solidi B **229**, r1 (2002).
[45]H. Jin, G. L. Zhao, and D. Bagayoko, J. Appl. Phys. **101**, 033123 (2007).
[46]R. B. Araujo, J. S. de Almeida, and A. Ferreira da Silva, J. Appl. Phys. **114**, 183702 (2013).
[47]F. Bechstedt and J. Furthmüller, J. Cryst. Growth **246**, 315 (2002).
[48]F. J. Piper, L. Colakerol, T. Learmonth, P.-A. Glans, K. E. Smith, F. Fuchs, J. Furthmüller, F. Bechstedt, T.-C. Chen, T. D. Moustakas, and J.-H. Guo, Phys. Rev. B **76**, 245204 (2007).
[49]D. Bagayoko and L. Franklin, J. Appl. Phys. **97**, 123708 (2005).
[50]L. F. J. Piper, T. D. Veal, P. H. Jefferson, and C. F. McConville, Phys. Rev. B **72**, 245319 (2005).
[51]P. Rinke, M. Scheffler, A. Qteish, M. Winkelnkemper, D. Bimberg, and J. Neugebauer, Appl. Phys. Lett. **89**, 161919 (2006).
[52]S. P. Fu and Y. F. Chen, Appl. Phys. Lett. **85**, 1523 (2004).
[53]K. Seeger, *Semiconductor Physics* (Springer, New York, 2002).
[54]H. Ahn, Y.-P. Ku, Y.-C. Wang, C.-H. Chuang, S. Gwo, and C.-L. Pan, Appl. Phys. Lett. **91**, 163105 (2007).